

Automatic arc discharge technology for inscribing long period fiber gratings

GUOLU YIN,^{1,2} JIAN TANG,¹ CHANGRUI LIAO,¹ AND YIPING WANG^{1,*}

¹Key Laboratory of Optoelectronic Devices and Systems of Ministry of Education and Guangdong Province, College of Optoelectronic Engineering, Shenzhen University, Shenzhen 518060, China

²Aston Institute of Photonic Technologies, Aston University, Birmingham B4 7ET, UK

*Corresponding author: ypwang@szu.edu.cn

Received 7 March 2016; revised 17 April 2016; accepted 17 April 2016; posted 18 April 2016 (Doc. ID 260775); published 10 May 2016

We experimentally demonstrate an automatic arc discharge technology for inscribing high-quality long period fiber gratings (LPGs) with greatly improved inscription efficiency for single mode fiber (SMF) and photonic crystal fiber (PCF). The proposed technology was developed by implementing an embedded program in a commercial fusion splicer. In addition, the improved technology employs an ultraprecision motorized translation stage, and the tensioning mass required by conventional technology was eliminated. While hundreds of arc discharges are generally required by conventional technology, only 30 and 60 arc discharges were required to inscribe LPGs with dip attenuations of 30 and 20 dB for SMF and PCF, respectively. © 2016 Optical Society of America

OCIS codes: (060.2340) Fiber optics components; (060.2310) Fiber optics; (050.2770) Gratings.

<http://dx.doi.org/10.1364/AO.55.003873>

1. INTRODUCTION

Long period fiber gratings (LPGs) have been increasingly employed in a wide variety of applications, including optical fiber sensors [1,2], wavelength rejection filters [3], mode converters [4], and optical polarizers [5]. LPGs were first inscribed by the exposure of photosensitive fibers to UV radiation [3]. However, several non-UV methods, such as CO₂ laser irradiation [6,7], femtosecond laser irradiation [8], ion-beam irradiation [9], periodic micro-bends [10], periodic tapering [11], and electric arc discharge technology [12], were subsequently developed for inscribing LPGs in both photosensitive fibers and nonphotosensitive fibers. Among these methods, electric arc discharge technology introduced in the 1990s has drawn wide attention owing to its simplicity, the absence of requirements for expensive laser equipment, thermal stability of the resulting LPGs, and its applicability to nearly any type of glass fiber.

However, conventional arc discharge technology has been typically executed manually over the past 20 years, the drawbacks of which have tended to obstruct the fuller development of this technology. First, a manual system is comprised mainly of a fusion splicer, a translation stage, and a fiber tensioning mass. These separate components function independently of each other, so that establishing and preserving the alignment of the system represents a serious challenge for inscribing high-quality LPGs. Second, the precision of the translation stage employed is generally on the order of 0.1 μm but can even be as low as 1.25 μm, which greatly undermines the precision of the resulting grating pitch [13,14]. Last, but not least,

the system itself imposes irreconcilable contradictions between the quality of the resulting LPGs and the inscription efficiency due to the use of the fiber tensioning mass. In conventional arc discharge technology, a mass must be attached at one end of the fiber for applying the requisite tension to straighten the fiber. When employing a light mass, e.g., 2.0 g, a low arc discharge current, and a short-duration arc discharge to inscribe LPGs, high-quality LPGs can be obtained with clean transmission spectra and low insertion losses. However, the gentle fabrication condition results in a weak refractive index modification; thus, the inscription efficiency of LPGs is very low. Therefore, hundreds of arc discharges are required for single mode fiber (SMF) [15–17] and photonic crystal fiber (PCF) [18–20]. Contrarily, LPGs can be inscribed with only tens of arc discharges when employing a heavy mass, e.g., 36.3 g, but the resulting LPGs are usually accompanied with obvious physical deformation, i.e., fiber taper. For example, a 20% decrease of the fiber diameter was observed when employing a mass of 36.3 g [21]. The resulting fiber tapers make the core and cladding regions locally and periodically reduced, which results in the periodic variation of the effective refractive indices in addition to the refractive index variation generated by the local thermal modulation, which is according to the discharge current and duration [11]. Therefore, the fiber tapers can enhance the coupling strength and reduce the number of arc discharges to improve the inscription efficiency. However, fiber tapers in the LPGs naturally increase the insertion loss [22,23] and also leads to variations in the positions of resonant dips due to the decreased

difference between the effective refractive indices of the fundamental mode and the cladding modes [24]. In addition, the reproducibility error of the taper is as great as $5\ \mu\text{m}$ [25], which significantly reduces the reproducibility of the LPFGs. Moreover, application to PCFs rather than SMFs exacerbates this problem due to the inclusion of air holes in the structure of a PCF [26].

In the present study, we developed an automatic arc discharge technology to simultaneously improve the quality and inscription efficiency of LPFGs for SMF and PCF. The key aspect promoting the success of this technology is the incorporation of a fully automatic inscription program in an integrated inscription system. Furthermore, the improved technology employs an ultraprecision motorized translation stage with a precision of 10 nm, and the fiber tensioning mass required by conventional technology is eliminated.

2. FABRICATION TECHNOLOGY

A schematic of our proposed technology is shown in Fig. 1(a), which employs a commercial fusion splicer system (ARCMaster FSM-100P+, Fujikura) to inscribe LPFGs. Figure 1(b) presents a photograph of the developed system. The system employs three motors to drive the corresponding transmission stages in the Z direction, namely, the ZL, ZR, and SWEEP motors. The parameters of the three motors are listed in Table 1. It is noted that all motors have a precision of 10 nm, and both transmission stages controlled by the ZL and ZR motors are simultaneously translated with operation of the SWEEP motor. For conducting LPFG inscription, the ZL and ZR motors are first

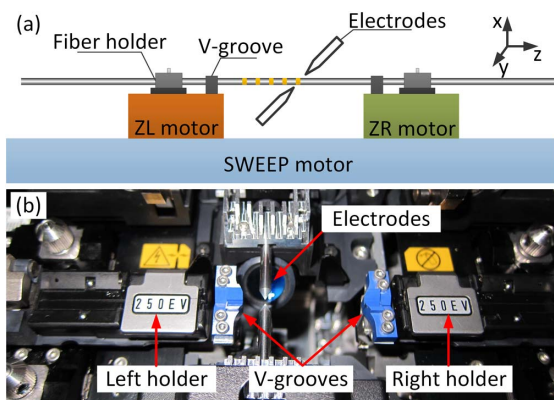


Fig. 1. Proposed arc discharge technology for inscribing LPFGs. (a) Diagram. (b) Photograph of the arc discharge technology employing a commercial fusion splicer (FSM-100P+).

Table 1. Parameters of the Three Motors Employed in the FSM-100P+ System

Motor	Location	Direction	Range (mm)	Precision (nm)
ZL	Left side	-Z	-18	10
ZR	Right side	+Z	+18	10
SWEEP	Under ZL & ZR	+/-Z	+/- 18	10

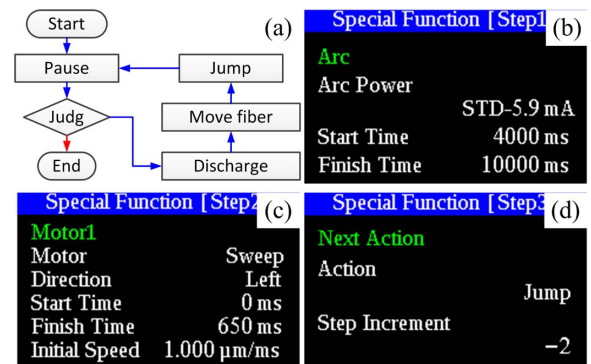


Fig. 2. LPFG inscription program: (a) program flow chart; (b) first step (discharge); (c) second step (move fiber); (d) third step (jump).

operated to prepare an adequate separation between the left and right fiber holders affixed to the top of the ZL and ZR transmission stages, as shown in Fig. 1(b). Second, a fiber with a short unjacketed section in the middle is fixed by the left and right fiber holders. The ZL and ZR motors are activated to apply a tiny tension to just straighten the fiber. Third, the inscription process is performed automatically and stopped once a desired LPFG transmission spectrum is obtained based on periodical monitoring of the transmission spectrum using an optical spectral analyzer (AQ6370C, Yokogawa Electric Corp.) with a wavelength resolution of 20 pm. By eliminating the tensioning mass employed in conventional technology, the source of physical deformation is also alleviated because any elongation of the fiber at the point of discharge has the effect of reducing the tension.

Automatic LPFG inscription was conducted by means of a program which we implemented in the splicer system. The program executes periodical point-to-point discharge according to the program flow chart shown in Fig. 2(a). The program is comprised of the three main steps illustrated on the right side of Fig. 2(a). The first step performs arc discharge for a period of time, e.g., 6 s. The arc discharge time is determined by subtracting the Start Time from the Finish Time, as shown in Fig. 2(b). The second step moves the fiber according to the grating pitch, e.g., $650\ \mu\text{m}$, along its longitudinal axis via the SWEEP motor, as shown in Fig. 2(c). Here, the grating pitch is determined by multiplying the Finish Time by the Initial Speed. The third step jumps to the first step for the next arc discharge, as shown in Fig. 2(d). A time gap, e.g., 4 s, is implemented prior to initiating Step 1, as indicated by the Start Time shown in Fig. 2(b). The time gap allows a user to measure the transmission spectrum of the LPFG and judge whether to continue the program or stop, as illustrated on the left side of Fig. 2(a). The program is automatically executed by pushing the button labeled SET on the splicer panel and stopped by pushing the button labeled RESET. Furthermore, the program is transferable to any FSM-100 series splicer for LPFG inscription.

3. EXPERIMENTAL RESULTS

The SMF employed in the experiments was the FuIIBand Plus low loss single mode fiber from Yangtze Optical Fiber and

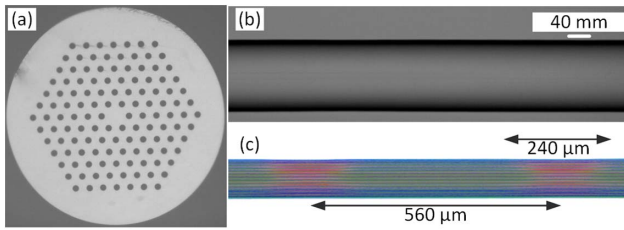


Fig. 3. (a) Cross-sectional image of the PCF, optical microscope images of LPFGs inscribed in (b) SMF and (c) PCF.

Cable Co., Ltd., which is denoted as YOFC-SMF in this paper. The PCF employed was ESM-12 with a core diameter of about 12 μm from NKT Photonics, Inc. In the PCF, air holes of 3.3 μm diameter are arranged in a hexagonal pattern with a pitch of 7.4 μm, as shown in Fig. 3(a). Figures 3(b) and 3(c) present optical microscope images of short segments of SMF and PCF subjected to the inscription process, which display no visible physical deformations. The red and green sections represent regions of arc discharge and no discharge, respectively. The length of the arc discharge region is around 240 μm, and the distance between the centers of two adjacent red regions, i.e., grating pitch, is about 560 μm, which agrees with the program settings employed.

A. Influence of the Arc Discharge Parameters

Compared with conventional arc discharge technology, complications associated with the tensioning mass have been avoided by the proposed technology. Hence, the only remaining factors that influence the quality and inscription efficiency are the arc discharge parameters given as the arc current (I_{arc}) and the arc duration (T_{arc}). Therefore, we first analyzed the influence of the arc discharge parameters on the grating growth for the SMF by inscribing several gratings with the same grating pitch (Λ) of 650 μm. These gratings have several resonant dips in the transmission spectra. The values of maximum dip attenuation (MA_{dip}) were plotted with respect to number of arc discharges (N) in Fig. 4(a). It is found that the resonant dips grew gradually when I_{arc} was fixed at 13 mA. The growing velocity becomes faster and faster when T_{arc} was increased from 5 to 8 s. Once T_{arc} reached 8 s, if I_{arc} was increased from 13 to 13.8 mA, the resonant dip grew dramatically.

Figures 4(b) and 4(c) show the transmission spectra evolutions with respect to increasing N for two LPFGs, i.e., LPFG₁ and LPFG₂, which were fabricated with $I_{arc} = 13$ mA and $T_{arc} = 6$ s, and $I_{arc} = 13.8$ mA and $T_{arc} = 8$ s, respectively. Compared LPFG₁ with LPFG₂, the MA_{dip} of LPFG₁ increased gradually and approached to a value of ~30 dB at $N = 27$, whereas that of LPFG₃ increased dramatically and attained a value of 25 dB at $N = 11$. It could therefore be concluded that the inscription efficiency could be further improved by increasing I_{arc} and T_{arc} . However, the larger values of I_{arc} and T_{arc} also increased the insertion loss (IL) from 0.2 to 1 dB and increased the 3 dB bandwidth from 42 to 100 nm. The grating performance with different arc discharge parameters is summarized in Table 2. To balance the IL, FWHM, and inscription efficiency, we selected values for I_{arc} and T_{arc} of 13 mA and 6 s, respectively, to inscribe LPFGs in SMF.

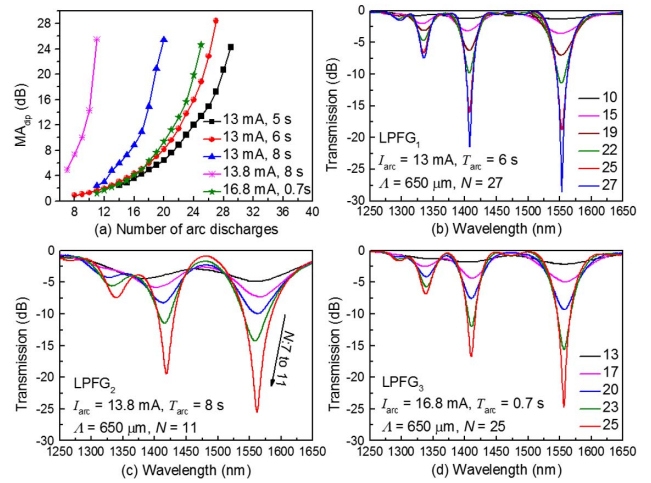


Fig. 4. (a) Comparison of maximum dip attenuation evolution of gratings inscribed by different arc discharge parameters; transmission spectra evolutions of LPFGs inscribed with different arc discharge parameters in SMF with equivalent grating pitches of 650 μm; (b) LPFG₁ with arc current of 13 mA and duration of 6 s; (c) LPFG₂ with arc current of 13.8 mA and duration of 8 s; (d) LPFG₃ with arc current of 16.8 mA and duration of 0.7 s.

Table 2. Influence of Arc Discharge Parameters on Grating Performance in SMF with $\Lambda = 650$ μm

I_{arc} (mA)	T_{arc} (s)	IL (dB)	MA_{dip} (dB)	FWHM (nm)	N
13	5	0.2	24	39	29
13	6	0.2	30	42	27
13	8	0.6	25	58	21
13.8	8	1	25	100	11
16.8	0.7	0.4	24	51	25

Additionally, we inscribed LPFG₃ with a huge I_{arc} of 16.8 mA and a tiny T_{arc} of 0.7 s, as show in Fig. 4(d). The MA_{dip} of LPFG₃ was also plotted with respect to N in Fig. 4(a). Though LPFG₃ has a much faster cooling rate than that of LPFG₁, the resonant dip of LPFG₃ has a similar growing tendency with that of LPFG₁. This indicates that the faster cooling rate does not induce much refractive index modulation in SMF due to the glass structure change, and the refractive index modulation in SMF is mainly generated by the residual stress relaxation due to the local thermal heating. This result agrees well with the study of refractive index profile changes caused by arc discharges with large arc current and tiny short arc duration [27].

Finally, we tested the reproducibility by fabricating a series of LPFGs with Λ of 650 μm and the same arc discharge parameters. Figure 5 illustrates the transmission spectra of three typical gratings in all fabricated LPFGs. LPFG₄ and LPFG₅ have the resonant dips, which locate in the shortest wavelength of 1553.36 nm and the longest wavelength of 1556.14 nm, thus indicating the reproducibility of the resonant wavelength is around ± 1.39 nm. LPFG₆ has a resonant dip located near the dip of LPFG₄. The separation is as low as 0.47 nm.

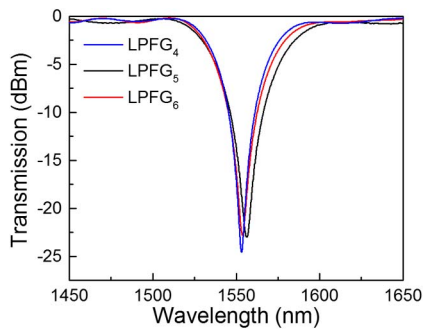


Fig. 5. Transmission spectra of three typical LPFGs with Λ of 650 μm and the same arc discharge parameters.

Therefore, it can be concluded that the proposed technology can fabricate LPFGs with high reproducibility.

It is more difficult to inscribe high-quality LPFGs in PCF than SMF because the softening point of the PCF is generally lower than that of the SMF, and the surface tension will overcome the viscosity of the glass and cause the cylindrical air holes in the PCF to collapse. To avoid collapse, the arc discharge parameters must be carefully optimized. After several trials, the values of I_{arc} and T_{arc} were selected as 13.9 mA and 0.7 s, respectively.

Table 3 lists the arc discharge parameters employed in all subsequent discussion. To demonstrate the quality of the resulting LPFGs and the inscription efficiency of the proposed system, a large number of LPFG samples were fabricated in both SMF and PCF using the proposed arc discharge technology in conjunction with the optimized parameters. Details regarding the resulting LPFGs in SMF and PCF are presented separately, and the results are compared with LPFGs fabricated by conventional arc discharge technology in the following three subsections, respectively.

B. LPFGs in SMF

A large number of LPFG samples with different values of Λ , which varied from 360 to 750 μm with an interval of 10 μm , were fabricated. Figure 6 shows the transmission spectra of five LPFGs with Λ values of 380, 450, 550, 650, and 750 μm . It is found that all gratings exhibited good quality with clean spectra, large values of MA_{dip} up to 30 dB, and low ILs of ~ 0.2 dB. To ensure high quality, the value of N varied from 23 to 34. This data is summarized in Table 2. Here, the minimum Λ achieved was 360 μm , which is comparable with the value of 345 μm reported elsewhere [17]. The small difference may be caused by the use of different electrodes in the respective experiments.

To determine what cladding modes were involved in the resonant dips, the near mode fields of the resonant dips for

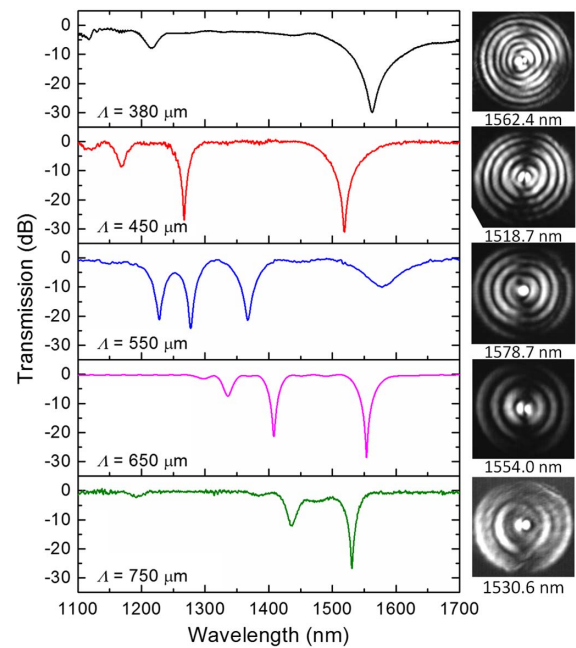


Fig. 6. Transmission spectra of LPFGs inscribed in SMF with grating pitches of 380, 450, 550, 650, and 750 μm . The insets represent the near mode fields corresponding to the resonant dips of the five LPFGs at 1562.4, 1518.7, 1578.7, 1554.0, and 1530.6 nm, respectively.

the five LPFGs with Λ values of 380, 450, 550, 650, and 750 μm were evaluated. To this end, a tunable laser (81960A, Agilent Technologies) with a tunable wavelength range from 1505 to 1630 nm was connected to one end of an LPFG sample as a single wavelength light source, and the other end of the LPFG sample was cleaved at the last grating period to observe the near mode field using a near-infrared camera. The insets given in Fig. 6 present the near mode fields observed at the longest resonant wavelength for each of the five LPFGs, i.e., 1562.4, 1518.7, 1578.7, 1554.0, and 1530.6 nm, respectively. The intensity distributions of the near mode field patterns indicate that the observed resonant dips of the five LPFGs correspond to coupling from the fundamental LP_{01} mode to the LP_{17} , LP_{16} , LP_{15} , LP_{14} , and LP_{13} cladding modes, respectively. These results indicate that the arc discharge results in inhomogeneous refractive index modulation in the fiber cross section, and the arc discharge induced LPFGs in standard SMF couple light to the antisymmetric cladding modes.

The inhomogeneous refractive index modulation would make the grating sensitive to the input state of polarization (SOP). Hence, we used an all optical parameter system to measure the transmission spectra of the LPFG at the slow axis and the fast axis. The measurement system was constructed by the tunable laser used for measuring the near mode field, a polarization synthesizer (Agilent N7786B), and a high power meter (Agilent N7744A). Figure 7 illustrates the result of the grating with Λ of 650 μm . Due to the limitation of the wavelength range of the tunable laser, we only measured the transmission spectra with the resonant dip corresponding to the LP_{14} cladding mode. It is found that the resonant wavelength has a separation of ~ 1.2 nm between the two orthogonal SOPs.

Table 3. Parameters of the Arc Discharge and LPFGs

Fiber Type	Arc Parameters		Grating Parameters			
	I_{arc} (mA)	T_{arc} (s)	IL (dB)	MA_{dip} (dB)	Λ (μm)	N
SMF	13	6	0.2	~ 30	360–750	23–34
PCF	13.9	0.7	0.5	~ 20	480–580	60–72

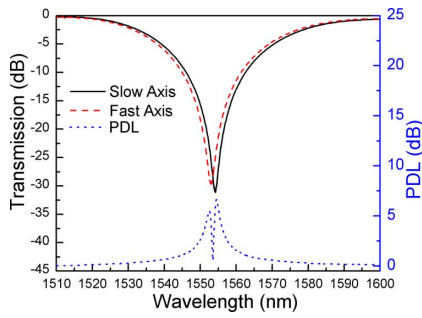


Fig. 7. Transmission spectra at the slow axis and fast axis for the LPFG with Λ of 650 μm , and the polarization dependent loss between the two axes.

The resonant wavelength separation results from the different effective refractive index of LP_{14} cladding mode at the two orthogonal SOPs. Furthermore, we can obtain the polarization dependent loss (PDL) by subtracting the transmission in the slow axis from the one in the fast axis and taking the absolute value. The maximum PDL is around 6.7 dB, which is comparable with that of the LPFGs fabricated by the traditional arc discharge technique [28].

C. LPFGs in PCF

We inscribed six LPFG samples in PCF with different values of Λ of 480, 500, 520, 540, 560, and 580 μm . The value of N varied within the range of 60 to 72. This data is summarized in Table 3. For each LPFG sample, arc discharge was terminated once the MA_{dip} attained a value greater than 20 dB. Any further increase in N would result in a diminishing resonant dip due to overcoupling from the cladding mode to the fundamental mode. Figure 8(a) shows the transmission spectra of an LPFG with $\Lambda = 560 \mu\text{m}$, and Fig. 8(b) illustrates the MA_{dip} with respect to N . The figure indicates that the MA_{dip} increased gradually with the increasing of N . The value of MA_{dip} was only 1 dB at $N = 20$ and then approaches a value of ~ 20 dB with a low IL of 0.5 dB at $N = 60$ dB. Because the PCF is made of pure silica, the thermal heating cannot generate a refractive index variation due to the residual stress relaxation, and the refractive index modulation in PCF mainly results from the glass structure change caused by the fast local heating-cooling process [19].

The transmission spectra of the six LPFGs in PCF are illustrated in the bottom panel of Fig. 9(a). The corresponding

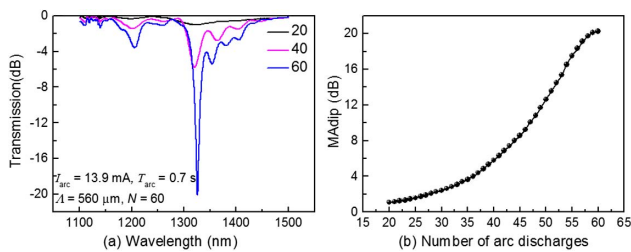


Fig. 8. LPFG inscribed in PCF with a grating pitch of 560 μm (a) transmission spectra at 20, 40, and 60 arc discharges. (b) Maximum dip attenuation evolution with respect to the number of arc discharges.

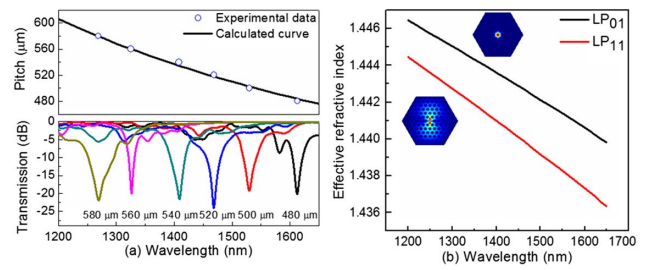


Fig. 9. (a) Six LPFG samples inscribed in PCF (bottom panel), and the relationship between the resonant wavelength and the grating pitch (top panel). (b) Effective refractive indices of LP_{01} core mode and LP_{11} cladding mode in the PCF. Inset: mode profiles of LP_{01} and LP_{11} .

resonant wavelengths are plotted with respect to Λ in the up panel of Fig. 9(a). On the other hand, we calculated the phase-matching curve based on the finite element method. Figure 9(b) illustrates the effective refractive indices of the LP_{01} core mode and LP_{11} cladding mode in the wavelength range from 1200 to 1650 nm. In PCF, light tends to spread to the air channels at longer wavelength; hence, the effective refractive index of the cladding mode rapidly decreases, leading to a negative slope of its phase-matching curve, as shown in the up panel of Fig. 9(a). As shown in Fig. 9(a), the experimental data matches well with the calculated curve. The figure further shows that the resonant wavelength of an LPFG in PCF decreases with increasing Λ , which is the opposite to that observed in LPFGs inscribed in SMF [29] and is also in agreement with previously reported results of LPFGs inscribed in PCF [19].

D. Comparison with LPFGs Fabricated by Conventional Arc Discharge Technology

To further emphasize the advantages of the proposed automatic arc discharge technology, Table 4 lists the primary characteristics of the LPFGs obtained in the present study in comparison with those of other reported LPFGs inscribed by conventional arc discharge technology. Comparison indicates that the value of N was reduced from 100–165 to 30 for LPFGs inscribed in SMF and from 94–120 to 60 for LPFGs inscribed in PCF, while attaining a reasonably equivalent or better MA_{dip} . Furthermore, the results of the proposed technology are comparable with LPFGs inscribed by CO_2 laser, while avoiding the necessity of repetitive scanning cycles required by CO_2 laser

Table 4. Comparison of LPFGs Inscribed by Various Arc Discharge Methods

Fiber Type	Λ (μm)	N	MA_{dip} (dB)	Ref.
Corning-SMF28	600	86	24	[30]
Corning-SMF28	345	108	32	[17]
N-doped SMF	250	100	13	[15,16]
B/Ge-doped SMF	221	165	24	[17]
YOFC-SMF	360–750	23–34	30	This paper
Ge-free PCF	550	100	15	[18]
Pure-silica PCF	350	120	11	[19]
LMA-10 PCF	400	94	12	[20]
ESM-12 PCF	480–580	60–72	20	This paper

inscription technology [5]. These results clearly indicate that our arc discharge technology greatly improved the quality of LPFGs and inscription efficiency simultaneously. Therefore, compared with LPFGs inscribed by conventional arc discharge technology reported elsewhere [15–20,30], the present results achieved the highest dip attenuation with the least number of arc discharges and the lowest insertion loss.

Additionally, we compared the LPFGs in SMF with our previous LPFGs inscribed by periodically tapering the fiber [29]. The taper section was created by synchronously stretching the fiber once arc discharge was done. Though the previous LPFG had an MA_{dip} of 30 dB, the taper section in the LPFG introduced a high IL of 1 dB. Furthermore, the taper technology is not suitable for inscribing LPFGs in PCF because it would make the air holes collapse and introduce a huge IL.

4. CONCLUSION

A promising arc discharge technology was proposed for fabricating LPFGs, and the technology was experimentally demonstrated to improve the quality and inscription efficiency of LPFGs inscribed in SMF and PCF. The proposed technology employed a fully automatic program in a commercial fusion splicer with a transmission stage having a precision of 10 nm to control the grating pitch. In addition, the designed system fixed the fiber using two fiber holders rather than a single holder and a tensioning mass, which is typical of conventional technology. As a result, the fabrication of LPFGs in SMF and PCF, respectively, required only 30 and 60 arc discharges, which resulted in resonant dips of 30 and 20 dB and insertion losses of 0.2 and 0.5 dB in SMF and PCF, respectively.

FUNDING

National Natural Science Foundation of China (NSFC) (61377090, 61405128, 61425007, 61575128); China Postdoctoral Science Foundation funded project (2014M552227, 2015T80913).

REFERENCES

1. V. Bhatia and A. M. Vengsarkar, "Optical fiber long-period grating sensors," *Opt. Lett.* **21**, 692–694 (1996).
2. X. Zhong, C. Guan, G. Mao, J. Fu, Y. Liu, J. Shi, and L. Yuan, "Bending characteristics of a long-period fiber grating in a hollow eccentric optical fiber," *Appl. Opt.* **54**, 7879–7883 (2015).
3. A. M. Vengsarkar, P. J. Lemaire, J. B. Judkins, V. Bhatia, T. Erdogan, and J. E. Sipe, "Long-period fiber gratings as band-rejection filters," *J. Lightwave Technol.* **14**, 58–65 (1996).
4. C. D. Poole, H. M. Presby, and J. P. Meester, "Two mode fiber spatial mode converter using periodic core deformation," *Electron. Lett.* **30**, 1437–1438 (1994).
5. Y. Wang, L. Xiao, D. N. Wang, and W. Jin, "In-fiber polarizer based on a long-period fiber grating written on photonic crystal fiber," *Opt. Lett.* **32**, 1035–1037 (2007).
6. Y. Wang, "Review of long period fiber gratings written by CO₂ laser," *J. Appl. Phys.* **108**, 081101 (2010).
7. A. Harhira, F. Guay, M. Daigle, J. Lapointe, and R. Kashyap, "Long period fiber gratings fabricated with a CO₂ laser beam and phase mask," *Opt. Commun.* **283**, 4633–4638 (2010).
8. Y. Kondo, K. Nouchi, T. Mitsuyu, M. Watanabe, P. G. Kazansky, and K. Hirao, "Fabrication of long-period fiber gratings by focused irradiation of infrared femtosecond laser pulses," *Opt. Lett.* **24**, 646–648 (1999).
9. M. L. von Bibra, A. Roberts, and J. Canning, "Fabrication of long-period fiber gratings by use of focused ion-beam irradiation," *Opt. Lett.* **26**, 765–767 (2001).
10. H. Sakata and K. Yamahata, "Magnetic-force-induced long-period fiber gratings," *Opt. Lett.* **37**, 1250–1252 (2012).
11. M. S. Yoon, H. J. Kim, S. J. Kim, and Y. G. Han, "Influence of the waist diameters on transmission characteristics and strain sensitivity of microtapered long-period fiber gratings," *Opt. Lett.* **38**, 2669–2672 (2013).
12. S. G. Kosinski and A. M. Vengsarkar, "Splicer-based long-period fiber gratings," in *Optical Fiber Communication Conference and Exhibit, Technical Digest (IEEE, 1998)*, pp. 278–279.
13. G. Rego, P. V. S. Marques, J. L. Santos, and H. M. Salgado, "Arc-induced long-period gratings," *Fiber Integr. Opt.* **24**, 245–259 (2005).
14. A. Martinez-Rios, I. Torres-Gomez, D. Monzon-Hernandez, G. Salceda-Delgado, V. M. Duran-Ramirez, and G. Anzueto-Sanchez, "Random period arc-induced long-period fiber gratings," *Opt. Laser Technol.* **44**, 1176–1179 (2012).
15. E. M. Dianov, V. I. Karpov, M. V. Grekov, K. M. Golant, S. A. Vasiliev, O. I. Medvedkov, and R. R. Khrapko, "Thermo-induced long-period fibre gratings," in *European Conference on Optical Communications (IEEE, 1997)*, pp. 53–56.
16. V. I. Karpov, M. V. Grekov, E. M. Dianov, K. M. Golant, S. A. Vasiliev, O. I. Medvedkov, and R. R. Khrapko, "Mode-field converters and long-period gratings fabricated by thermo-diffusion in nitrogen-doped silica-core fibers," in *Optical Fiber Communication Conference and Exhibit, Technical Digest (IEEE, 1998)*, pp. 279–280.
17. M. Smietana, W. J. Bock, P. Mikulic, and J. Chen, "Increasing sensitivity of arc-induced long-period gratings—pushing the fabrication technique toward its limits," *Meas. Sci. Technol.* **22**, 015201 (2011).
18. G. Humbert, A. Malki, S. Fevrier, P. Roy, and D. Pagnoux, "Electric arc-induced long-period gratings in Ge-free air-silica microstructure fibres," *Electron. Lett.* **39**, 349–350 (2003).
19. K. Morishita and Y. Miyake, "Fabrication and resonance wavelengths of long-period gratings written in a pure-silica photonic crystal fiber by the glass structure change," *J. Lightwave Technol.* **22**, 625–630 (2004).
20. H. Dobb, K. Kalli, and D. J. Webb, "Measured sensitivity of arc-induced long-period grating sensors in photonic crystal fibre," *Opt. Commun.* **260**, 184–191 (2006).
21. G. Rego, O. Okhotnikov, E. Dianov, and V. Sulimov, "High-temperature stability of long-period fiber gratings produced using an electric arc," *J. Lightwave Technol.* **19**, 1574–1579 (2001).
22. L. A. García-de-la-Rosa, I. Torres-Gómez, A. Martínez-Ríos, D. Monzón-Hernández, and J. Reyes-Gómez, "Background loss minimization in arc-induced long-period fiber gratings," *Opt. Eng.* **49**, 065001 (2010).
23. F. Durr, G. Rego, P. Marques, S. L. Semjonov, E. M. Dianov, H. G. Limberger, and R. P. Salathe, "Tomographic stress profiling of arc-induced long-period fiber gratings," *J. Lightwave Technol.* **23**, 3947–3953 (2005).
24. O. V. Ivanov and G. Rego, "Origin of coupling to antisymmetric modes in arc-induced long-period fiber gratings," *Opt. Express* **15**, 13936–13941 (2007).
25. W. J. Bock, C. Jiahua, P. Mikulic, and T. Eftimov, "A novel fiber-optic tapered long-period grating sensor for pressure monitoring," *IEEE Trans. Instrum. Meas.* **56**, 1176–1180 (2007).
26. W. J. Bock, J. Chen, P. Mikulic, T. Eftimov, and K.-P. Michael, "Pressure sensing using periodically tapered long-period gratings written in photonic crystal fibres," *Meas. Sci. Technol.* **18**, 3098–3102 (2007).
27. F. Abrishamian, N. Dragomir, and K. Morishita, "Refractive index profile changes caused by arc discharge in long-period fiber gratings fabricated by a point-by-point method," *Appl. Opt.* **51**, 8271–8276 (2012).
28. G. M. Rego, J. L. Santos, and H. M. Salgado, "Polarization dependent loss of arc-induced long-period fiber gratings," *Opt. Commun.* **262**, 152–156 (2006).
29. G. Yin, Y. Wang, C. Liao, J. Zhou, X. Zhong, G. Wang, B. Sun, and J. He, "Long period fiber gratings inscribed by periodically tapering a fiber," *IEEE Photon. Technol. Lett.* **26**, 698–701 (2014).
30. G. Humbert and A. Malki, "Electric-arc-induced gratings in non-hydrogenated fibres: fabrication and high-temperature characterizations," *J. Opt. A* **4**, 194–198 (2002).